BNL-105949-2014-TECH

BNL-105949-2014-IR

Double Quarter Wave Crab Cavity Field Profile Analysis and Higher Order Mode Characterization

C. Marques

June 2014

Collider Accelerator Department

Brookhaven National Laboratory

U.S. Department of Energy

USDOE Office of Science (SC)

DISCLAIMER

BNL-105949-2014-IR

C-A/AP/520
June 2014

Double Quarter Wave Crab Cavity Field Profile Analysis and Higher Order Mode Characterization

C. Marques, B.P. Xiao, S. Belomestnykh

Collider-Accelerator Department
Brookhaven National Laboratory
Upton, NY 11973

Brookhaven National Laboratory
Collider Accelerator Department
C-A/AP/520
June 2014

Double Quarter Wave Crab Cavity Field Profile Analysis and Higher Order Mode Characterization*

C. Marques[1,2], B. P. Xiao[1], S. Belomestnykh[1,2]
[1] *Accelerator R&D Division, Brookhaven National Laboratory, Upton, NY 11973*
[2] *Physics and Astronomy Department, Stony Brook University, Stony Brook, NY 11790*

E-mail
Carlos.Marques@Alumni.StonyBrook.edu

Abstract

The Large Hadron Collider (LHC) is underway for a major upgrade to increase its luminosity by an order of magnitude beyond its original design specifications. This novel machine configuration known as the High Luminosity LHC (HL-LHC) will rely on various innovative technologies including very compact and ultra-precise superconducting crab cavities for beam rotation[1]. A double quarter wave crab cavity (DQWCC) has been designed at Brookhaven National Laboratory for the HL-LHC. This cavity as well as the structural support components were fabricated and assembled at Niowave. The field profile of the crabbing mode for the DQWCC was investigated using a phase shift bead pulling technique and compared with simulated results to ensure proper operation or discover discrepancies from modeled results and/or variation in fabrication tolerances. Higher-Order Mode (HOM) characterization was also performed and correlated with simulations.

*Work partly supported by the EU FP7 HiLumi LHC grant agreement No. 284404 and by the US DOE through Brookhaven Science Associates, LLC under contract No. DE-AC02-98CH10886 with the US LHC Accelerator Research Program (LARP). This research used resources of the National Energy Research Scientific Computing Center, which is supported by the US DOE under contract No. DE-AC02-05CH11231.

1 Introduction

The LHC operates with a non-zero crossing angle at the interaction region to alleviate parasitic collisions and permit the largest number of bunches. However luminosity is lost from a non-zero crossing angle due to the geometric factor of the rotated bunches. To remedy the rotation a transverse deflection from a crab cavity aligns bunches for a head-on collision and subsequently rotates bunches back to their original trajectory before entering the accelerator for normal operation. The transverse kick is delivered to the bunch using the so called crabbing mode. The crabbing mode and traversing bunch are synchronized when the bunch is located at the center of the cavity and the mode at the zero crossing of the time varying RF field. Since the center of the bunch is at the zero crossing of the time varying RF field it experiences no deflection while the head and tail of the bunch are kicked in opposite directions. Beam optics are used to keep the rotated bunches aligned until they reach the interaction point and then subsequently rotated back to their original configuration for normal accelerator operation. A DQWCC has been designed at Brookhaven National Laboratory for both vertical and horizontal crabbing of the beams at the HL-LHC and can be seen in Figure 1 [2]. To ensure proper operation and execution of fabrication the field of the crabbing mode was investigating along with characterization of HOMs.

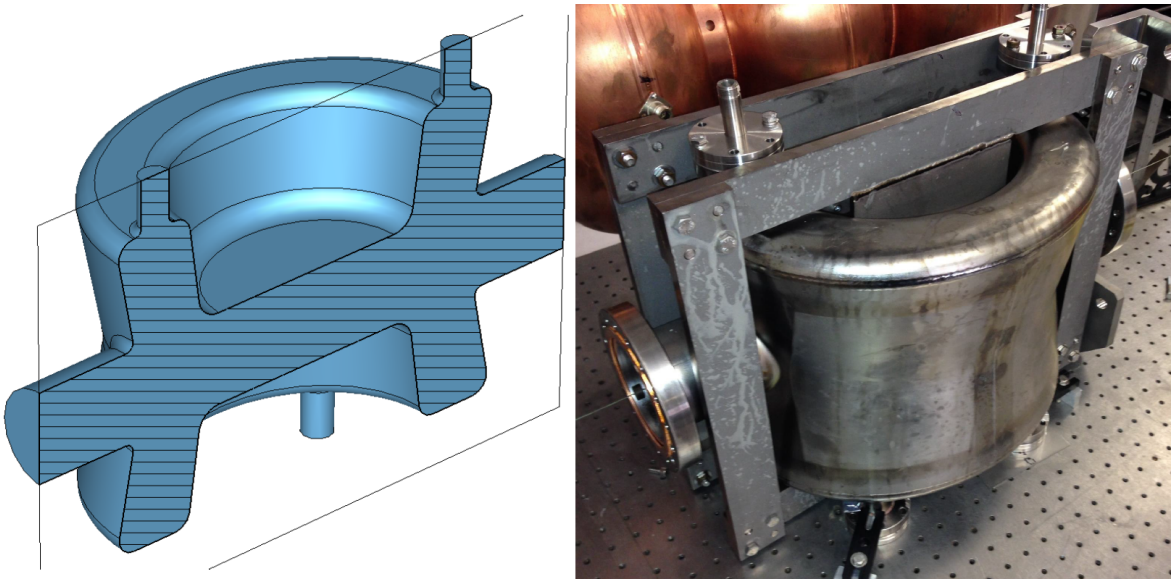

Figure 1: Cross sectional view of the simulated DQWCC design for the HL-HLC upgrade (left). Photograph of the niobium proof-of-principle DQWCC manufactured for the HL-HLC upgrade surrounded by a stiffening frame (right).

1.1 Experimental Setup

A perturbative phase shift method also known as the Slater method was used to measure the field profile of the DQWCC. This experiment used a copper cylinder (r=4mm, d=1.5mm) to perturb standing waves inside the DQWCC. The eigenfrequency shift is

given by the expression

$$\frac{\Delta\omega}{\omega_0} = F_H \frac{\mu_0 \mathbf{H}' \cdot \mathbf{H}'^*}{U} - F_E \frac{\epsilon_0 \mathbf{E}' \cdot \mathbf{E}'^*}{U}.$$

$\Delta\omega = \omega - \omega_0$, F_H and F_E are relative geometric factors which quantify the local coupling of the perturbed magnetic H' and electric E' fields respectively. The frequency shift from a perturbation using an S21 measurement from a network analyzer is

$$\frac{\Delta\omega}{\omega_0} \approx \frac{1}{2Q_L} \tan\Phi.$$

where $Q_L = 1/Q_0 + 1/Q_{\text{in}} + 1/Q_{\text{out}}$ and $Q_{\text{in}} = \omega U/P_{\text{in}}$, $Q_{\text{out}} = \omega U/P_{\text{out}}$ are the quality factors of a particular eigenfrequency for the input and output ports of the network analyzer respectfully. The mode excitation is critical to perform characterization measurements and hence locations of the input and output power (P_{in} and P_{out}) ports are also critical. The bead position is correlated to the measured phase shift given by an Agilent E5071C ENA network analyzer. By using the small angle approximation or by not excessively perturbing the standing waves while providing the best signal to noise, $\Phi \propto \mu_0|H|^2/2 - \epsilon_0|E|^2$ where the one half comes from the F_H geometric factor[3]. This is to good approximation for any geometric shape provided the perturbative bead is not an oblong shape and the absolute magnitude of the magnetic and electric fields need not be calculated. This suggests that the measured phase shift which is correlated to the bead position yields the absolute difference of the magnetic and electric field squared at that position resulting in a field profile. When using a strict dielectric perturbation such as teflon or micarta bead, the magnetic field contribution drops out; $\Phi \propto |E|^2$. The electric field profile for the DQWCC crabbing mode was also investigated and can be found in other work with similar results[4]. Higher Order Mode (HOM) characterization was also performed using a strict dielectric bead and can be found in Section 3.

The perturbative bead pull assembly used for measuring the absolute difference of the electric and magnetic field profile can be seen in Figure 2. The crab cavity was fixed between stepper motor driven translational stages capable of moving the suspended fishing line which supports the fixed dielectric bead in the X-Y plane. A computer controlled motor pulls the bead at a constant speed through the crab cavity in the Z axis yielding a full range of motion limited by the size of the beam tube openings and bead geometry. The beamtube for the DQWCC had a diameter of 8cm which limited the experiment to 35mm off axis measurements. A microcontroller was used to synchronize stepper motor movements with the network analyzer and correlate the bead position with the eigenfrequency shift. With the aid of the computer controlled stepper motors one step size would translate to 5.5×10^{-3} mm in either the X-Y axis and .165mm in the Z-axis. Not only would the microcontroller provide computer controlled precision and accuracy for the bead positioning but could also automate this measurement technique. More details of this assembly can be found elsewhere[4]. A cylindrical copper bead of dimensions r=4mm, d=1.5mm was used to perturb the magnetic and electric field lines of the crabbing mode and directly compare this perturbation to the measured phase shift given by the network analyzer. The orientation of the cylindrical bead influences

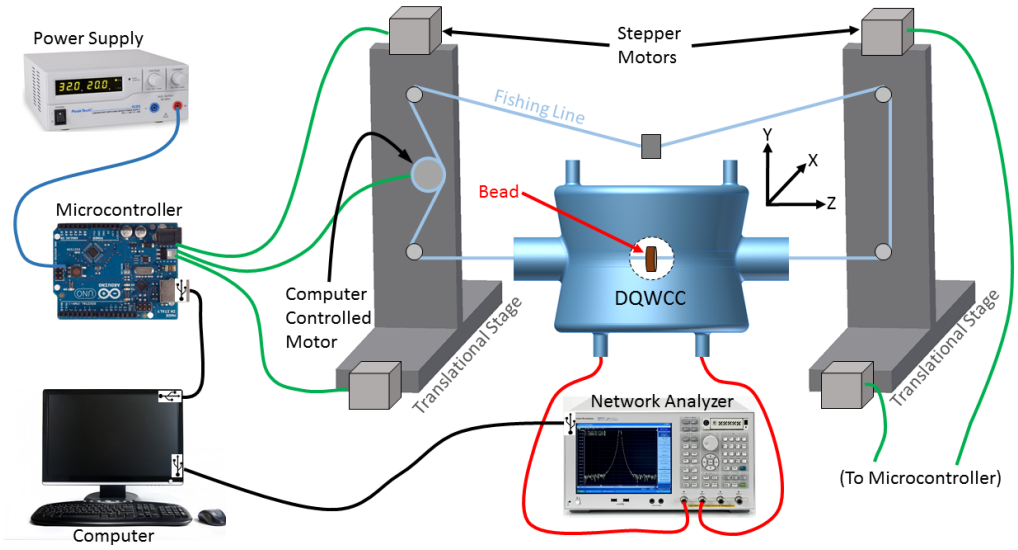

Figure 2: The perturbative bead pull assembly. Coordinate system used in this experiment can be found between the DQWCC and translational stage.

the perturbation on the field. For example if the electric field lines are normal to the disk plane then the electric field lines will terminate on both faces of the disk and will have the same form as if the electric field lines went right through the disk so that the disk in that orientation does not perturb the electric field. On the other hand if the disk is rotated such that the field lines lie on the disk plane then the bead offers a large perturbation. The opposite occurs for the magnetic field lines. If the magnetic field lines are normal to the disk plane then you have a large perturbation, etc. According to simulation results for the crabbing mode of the DQWCC, the magnetic field lines are maximum far away from the beam tubes and minimum along the beam tube axis while the electric field lines are maximum and perpendicular to the beam tube axis. Therefore the disk plane of the copper bead was oriented normal to the beam tube axis i.e. parallel to the electric field and can be seen in Figure 2.

2 Field Profile Results

Exploiting automation, the niobium DQWCC shown in Figure 1 was analyzed using longitudinal (z-axis) sweeps both on and off axis using one millimeter steps in the vertical (y-axis) and horizontal (x-axis) directions with respect to the beam tubes. The eigenfrequency shift collected by the network analyzer was correlated to the bead position. Simulations of the field components of the DQWCC were performed using CST Microwave Studio. Using a two parameter fit namely a proportionality constant and offset the collected data was compared to the simulated results. A chi squared analysis was performed on these data where

$$\chi^2 \equiv \sum^{i} \frac{1}{\sigma_i^2} \left(y_i - y(x_i)\right)^2,$$

σ_i^2 is the variance from the i^{th} dataset, y_i is the measured phase and $y(x_i)$ is the normalized simulated data. The results of the χ^2 fit versus position can be seen in Figure 3. The saddle like shape of the Figure 3 suggests a better goodness of fit with

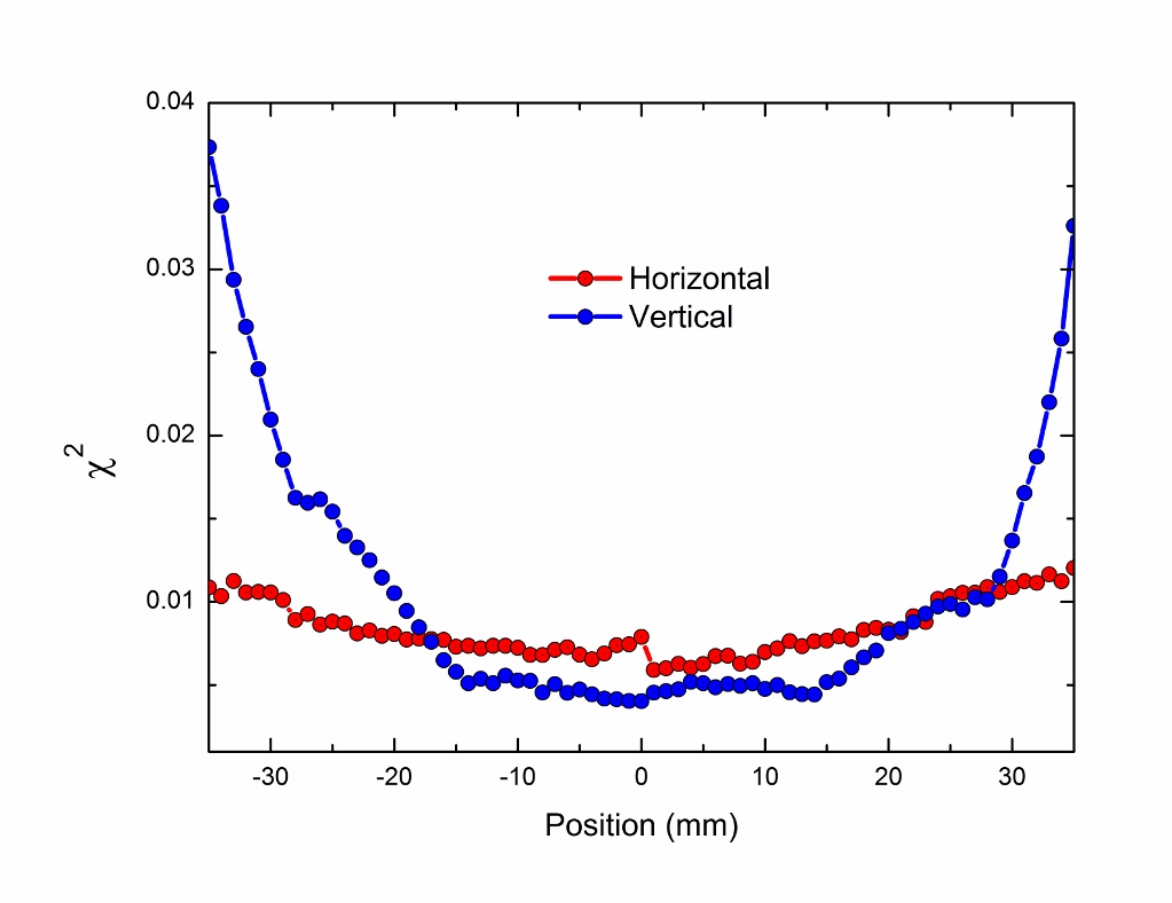

Figure 3: χ^2 fit versus off axis sweep position.

respect to the center of the beam tube than at the DQWCC edges. This is partially due to the obvious misalignment which can be seen in Figure 4 where the commensurate ear-like features are skewed along with the baseline and where misalignment weighs heavily on phase measurements for sections of higher field strength e.g. the beam tube edges. However these results yield an average χ^2 of 0.0084 and 0.0105 resulting in a probability of 99% level of confidence for both the horizontal and vertical configurations. The $\chi^2 =\sim 0.035$ or the 96% level of confidence on the edges of the of the DQWCC are consistent with a misalignment of a few millimeters and the mechanical survey of the structure[5]. The results of the field profiling for both the vertical and horizontal plane of the DQWCC can be found in Figures 5 and 6 respectfully. These results suggest an excellent agreement with the simulated DQWCC and consistency between the simulated prototype to fabricated structure.

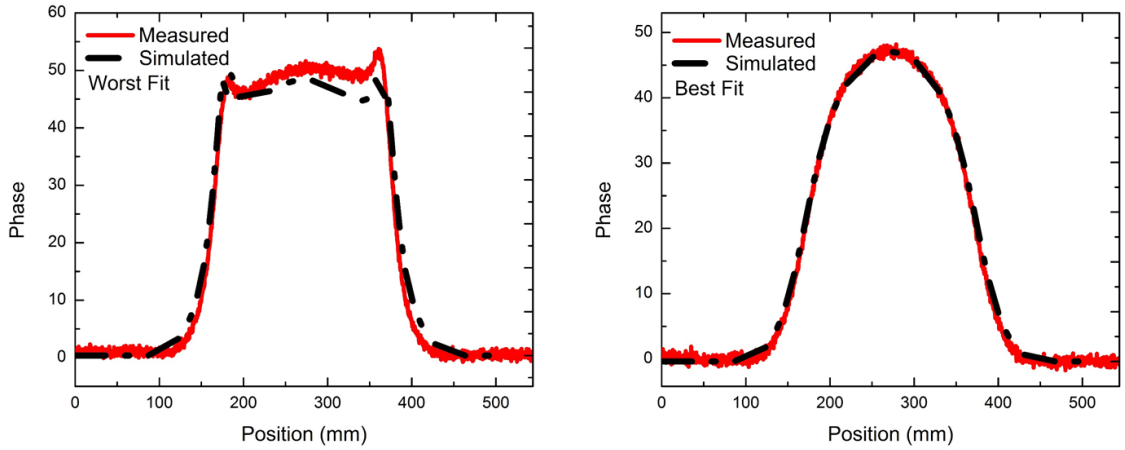

Figure 4: The left and right plots represent the measured and simulated field profile longitudinally through the DQWCC at -35mm and 0mm vertically off axis respectfully.

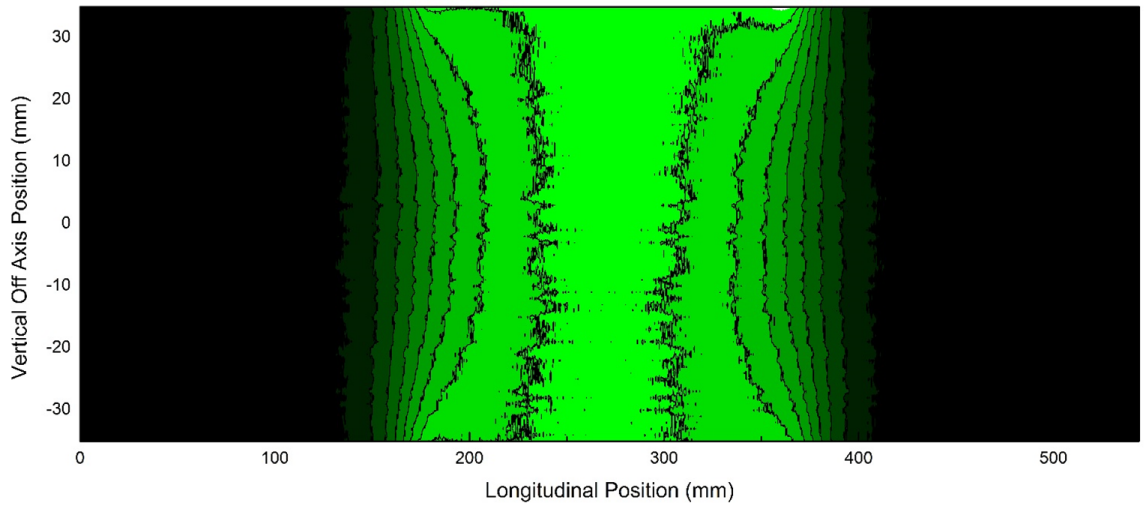

Figure 5: Phase profile or $\Phi \propto |H|^2/2 - |E|^2$ of the longitudinal sweeps vertically off axis with respect to the DQWCC beam tubes. Black and green regions represent a minimum and maximum field respectfully.

2-Port Cold (MHz)	2-Port Warm (MHz)	4-Port Warm (MHz)	Simulated Freq. (MHz)	Mode Type
403.93	403.25	403.25	400	Crabbing
581.44	579.9688	580.3375	576	TM Dipole
N/A	N/A	675.275	670	TEM Dipole
705.24	703.7188	703.95	700	TM Dipole
757.05	755.2813	755.4875	752	TEM Dipole
N/A	N/A	803.5375	800	TE Dipole
N/A	N/A	920.5625	915	TEM Dipole
958.73	956.375	N/A	946	TM Dipole
1082.97	1081.156	1080.625	1077	TEM Dipole
N/A	N/A	1104.375	1102	TE Dipole
1120.41	1118.281	1118.125	1113	TEM Dipole
N/A	N/A	1211.25	1202	TEM Dipole
1260.72	1258.531	1258.125	1246	TM Dipole
1298.82	1296.688	1296.25	1290	TEM Dipole
N/A	N/A	1358.125	1352	TE Dipole
1417.40	1414.25	1415	1408	TE Dipole
N/A	N/A	N/A	1409	TE Dipole
N/A	N/A	1495.625	1488	TEM Dipole
1561.97	1558.625	1558.75	1549	TEM Dipole
1579.23	1576.156	1576.25	1560	TM Dipole
N/A	1627.719	1627.5	1626	TE Dipole
N/A	N/A	N/A	1631	TE Dipole
1637.41	1633.906	1633.125	1634	TM Dipole
1670.46	1665.875	1666.25	1668	TM Dipole
1720.51	1717.438	1716.875	1706	TEM Dipole
N/A	N/A	N/A	1708	TE Dipole
N/A	N/A	1723.75	1725	TE Dipole
1768.65	1764.875	1765	1733	TEM Dipole
1783.26	1778.281	1779.375	1776	TM Dipole
1866.27	1861.813	1861.25	1863	TEM Dipole

Table 1: HOM eigenfrequency comparison in various configurations. N/A = Not Available.

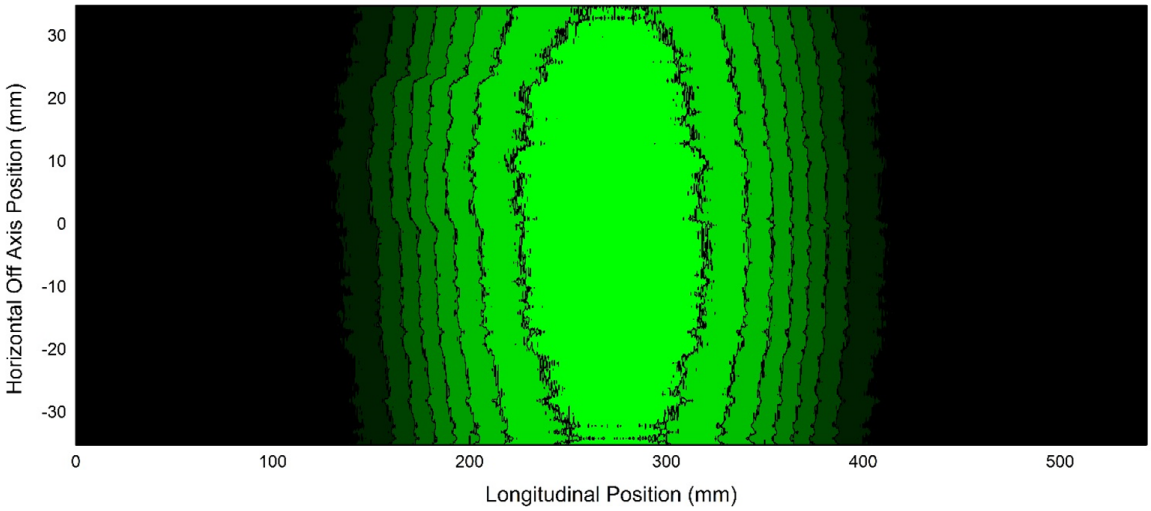

Figure 6: Phase profile or $\Phi \propto \mu_0|H|^2/2 - \epsilon_0|E|^2$ of the longitudinal sweeps horizontally off axis with respect to the DQWCC beam tubes. Black and green regions represent a minimum and maximum field respectfully.

3 HOM Characterization

HOMs were evaluated and characterized. The results of the eigenfrequency analysis are found in Table 1. Some modes were simply not found due to the lack of coupling from the fundamental power coupler (FPC) and pick up probe (PUP) configuration namely the modes located at 1.409, 1.631 and 1.708 GHz. The 2-Port configuration is the intended configuration for proper operation namely where the FPC and PUP are located at the top two ports of the DQWCC shown in Figure 1. The 4-Port configuration is when the FPC and PUP are connected to HOM coupler ports located on the opposite side. "Cold" data represents measurements taken when the DQWCC was submerged in liquid helium or at 4K while "warm" represents room temperature data or 300K. The results of these measurements show excellent agreement with respect to simulation but to ensure proper HOM identification, characterization was perform. HOMs were characterized by longitudinal scans both on and 20mm off axis in both the vertical and horizontal directions, followed by azimuthal scans 20mm off axis at points of interest specifically the center of the cavity (272mm) and a quarter of the total length into the cavity (136mm) or simply $L/4$. A cylinderical micarta bead of dimensions r=4mm, d=1.5mm was used to directly compare the phase profile of the DQWCC to the simulated absolute electric field squared mentioned above and the simulated and measured data was normalized for comparison. The results of these scans can be found in the BNL intranet network folder `\\bnl\c-adnas\crab_cavity\PoP DQWCC prototype\HOMs\HOM Characterization` as well as the following sections. The convention for identifying the different types of HOMs for example monopole, dipole, etc. was with respect to the transverse field through the beam tube and not to the coaxial-like feature of the DQWCC which is perpendicular to the beam propagation.

3.1 Mode at 580MHz

The first HOM is located at 580MHz and the results of the longitudinal characterization can be found in Figures 7, 8, 9. These scans suggest excellent correlation between the measured and simulated absolute electric field profile as well as a maximum field at $L/4$ and $3L/4$. Indeed the azimuthal measurements 20mm off axis also shows excellent correlation and can be seen in Figure 10. However the absolute electric field profile from the bead trajectory at the center and at $L/4$ is relatively unvarying and therefore the azimuthal measurement is mostly background and can also be seen in Figure 10.

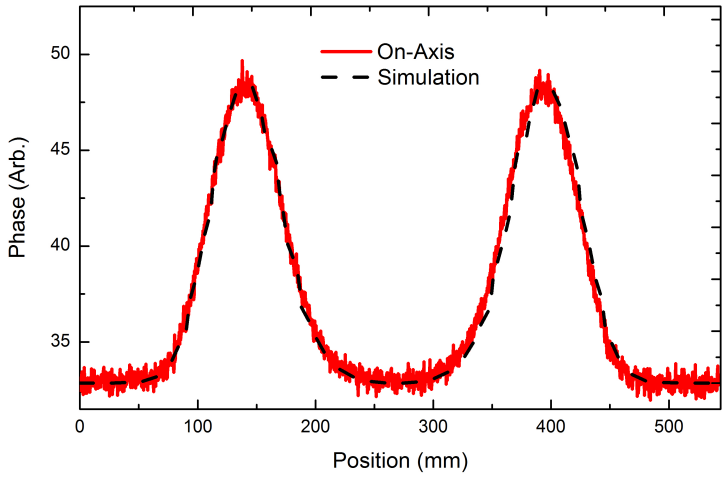

Figure 7: On-Axis longitudinal phase profile of the 580MHz mode.

3.2 Mode at 675MHz

Among the most weakly perturbed modes from our analysis is the mode located at 675MHz. The longitudinal as well as the azimuthal scans performed for characterization were in regions of minimum electric field and these results can be seen in Figures 11, 12, 14, 13, 15 and 16 where the signal to noise is quite poor. However the similar qualitative features of the simulation and measurement as well as the weak coupling to the bead implies an excellent prediction by simulation.

3.3 Mode at 704MHz

Simulations predicted that the mode located at 704MHz would have excellent coupling with the FCP and PUP located in the 2-port configuration. The longitudinal scans shows excellent signal to noise along with a maximum electric field at $L/4$ and $L3/4$. The results of these measurements can be seen in Figures 17, 19 and 18 where the

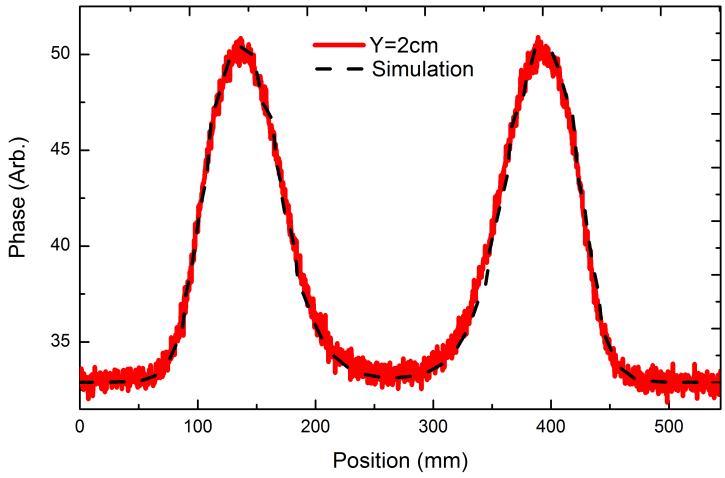

Figure 8: Longitudinal phase profile of the 580MHz mode 2cm vertically off axis.

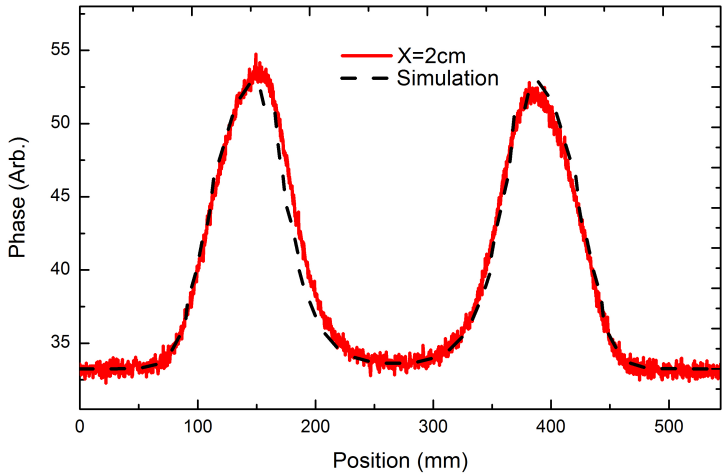

Figure 9: On-Axis longitudinal phase profile of the 580MHz mode 2cm horizontally off axis.

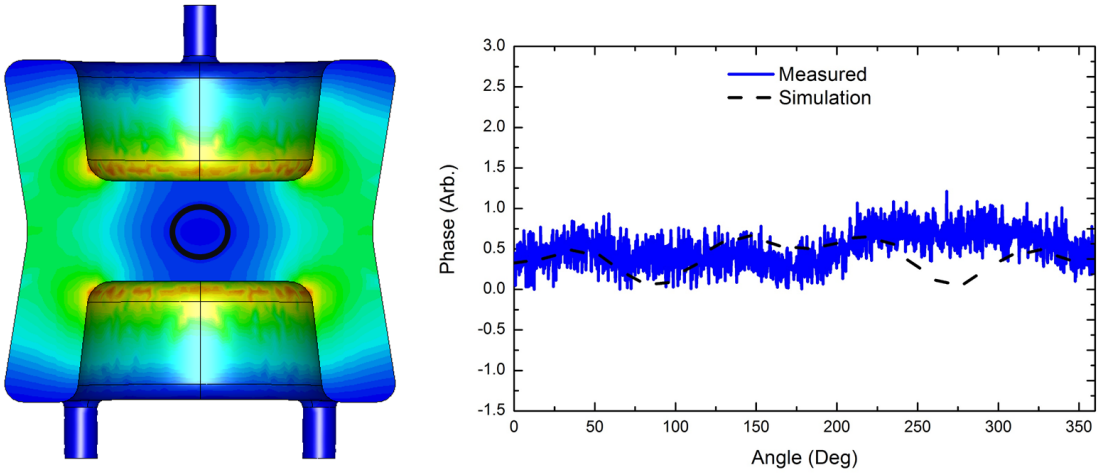

Figure 10: The left figure represents a simulated cross section of the absolute electric field profile of the 580MHz mode at center of the DQWCC. Red and blue contours represents maximum and minimum field respectfully. The black circle at the center is the trajectory of the bead starting from the left-most side in the counter-clockwise direction. The right figure is the measurement and simulation of the phase from that trajectory.

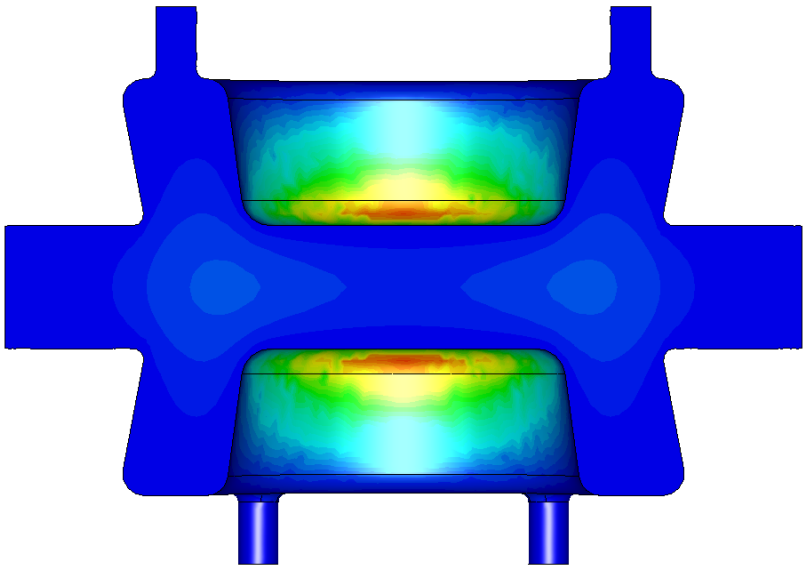

Figure 11: Longitudinal cross sectional view of the simulated absolute electric field profile of the 675MHz mode.

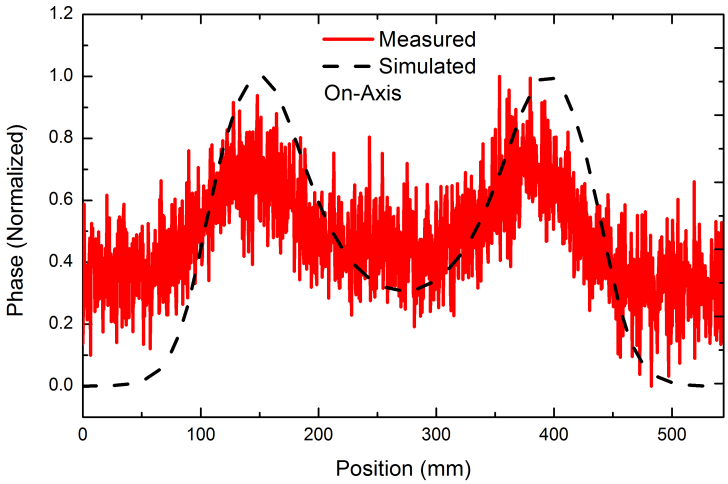

Figure 12: On-Axis longitudinal phase profile of the 675MHz mode.

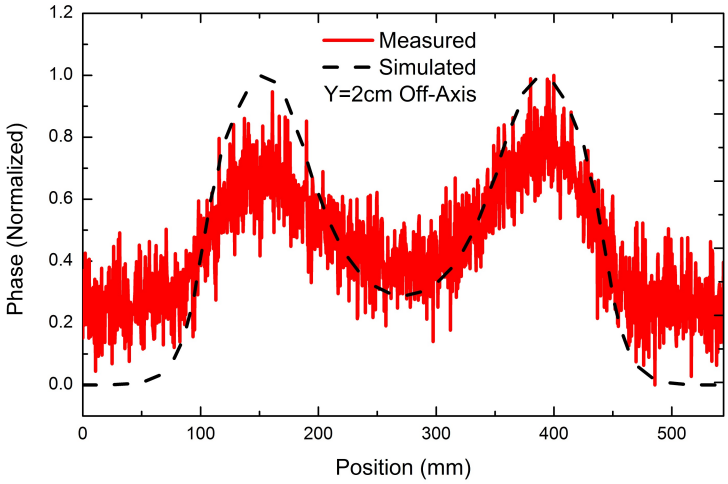

Figure 13: Longitudinal phase profile of the 675MHz mode 2cm vertically off axis.

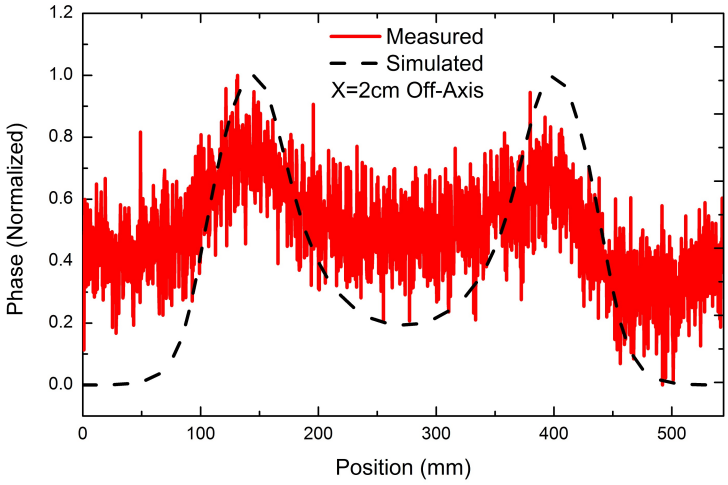

Figure 14: On-Axis longitudinal phase profile of the 675MHz mode 2cm horizontally off axis.

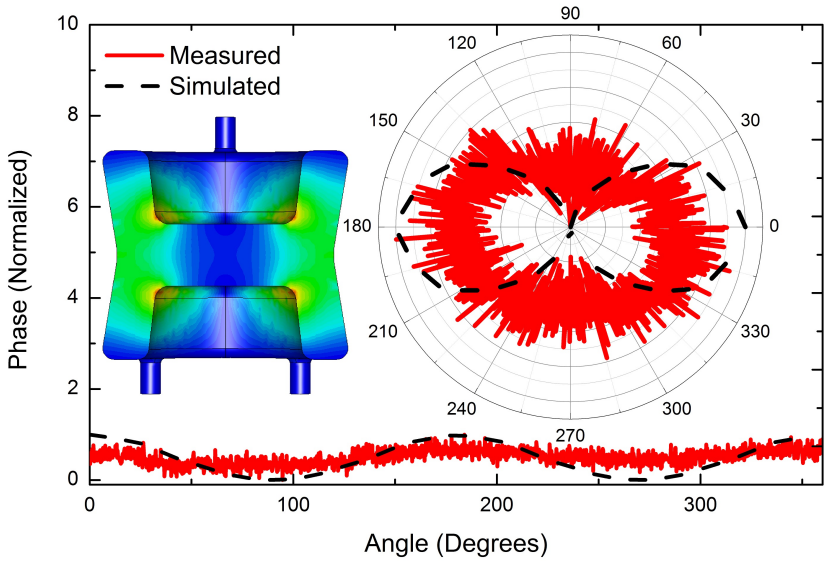

Figure 15: Azimuthal phase profile of the 675MHz mode at the center of the DQWCC. The insets are the transverse cross sectional view of the absolute electric field and the radial plot of the raw data.

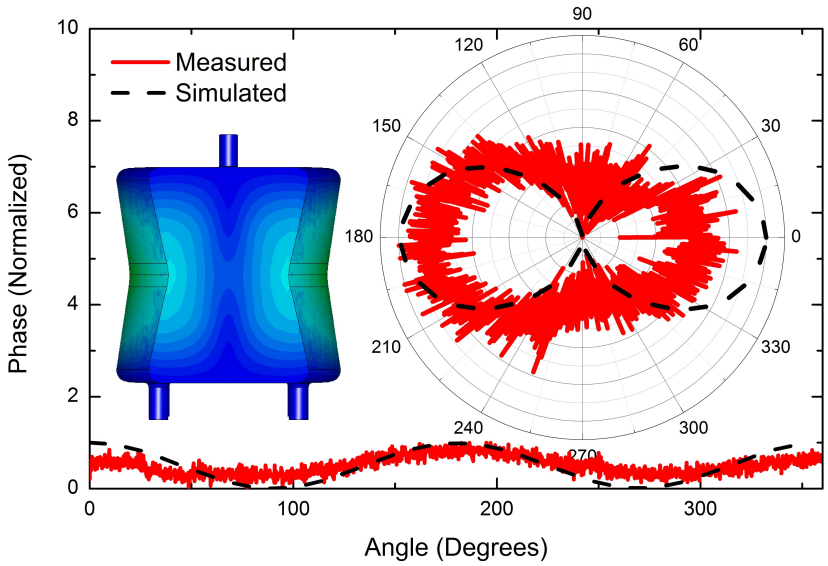

Figure 16: Azimuthal phase profile of the 675MHz mode at $L/4$ of the DQWCC. The insets are the transverse cross sectional view of the absolute electric field and the radial plot of the raw data.

correlation between simulation and measurement is excellent. On the other hand simulations also predicted very weak electric field at the center of the cavity which can be attributed to the small signal to noise ratio in Figure 20. The dipole characteristic about the beam axis is apparent from measurement.

3.4 Mode at 755MHz

The discrepancy of the simulated versus measured electric field of the 755MHz mode was alarming. A possible explanation for this discrepancy is that the bead perturbation was simply too large. As we know the $\Delta\omega \propto \tan\Phi$ and by using a small perturbation we shift $\Delta\omega$ slightly having a linear response or where $\Delta\omega \propto \Phi$. If the perturbation is large enough then the shift reaches a nonlinear region and indeed any measurement above a phase of ~ 45 degrees is in the nonlinear region. The effect of this phenomenon can be seen in Figures 21 and 23 where the measured data was trusted below a phase of 45 degrees and ignored above. If we disregard this detail the field profile is still qualitatively similar as seen in Figure 23. The azimuthal scan at $L/4$ shows excellent signal to noise as well as agreement to simulation. These results can be seen in Figure 24.

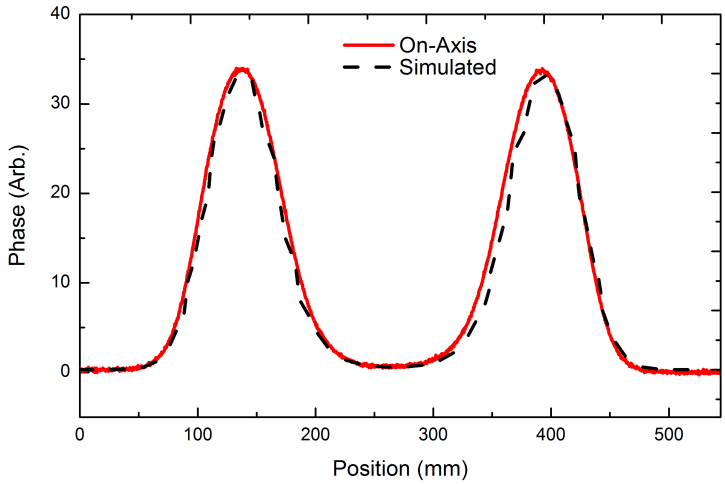

Figure 17: On-Axis longitudinal phase profile of the 704MHz mode.

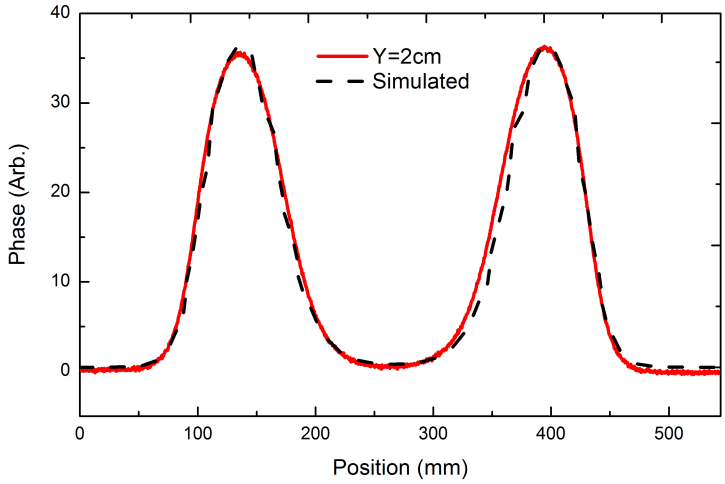

Figure 18: Longitudinal phase profile of the 704MHz mode 2cm vertically off axis.

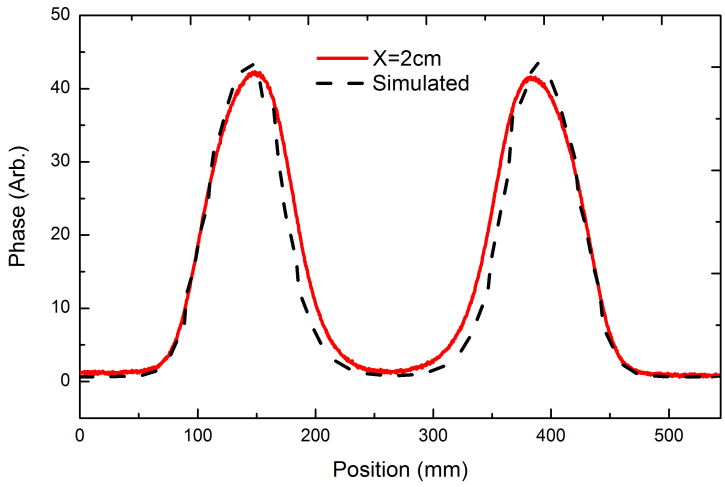

Figure 19: On-Axis longitudinal phase profile of the 704MHz mode 2cm horizontally off axis.

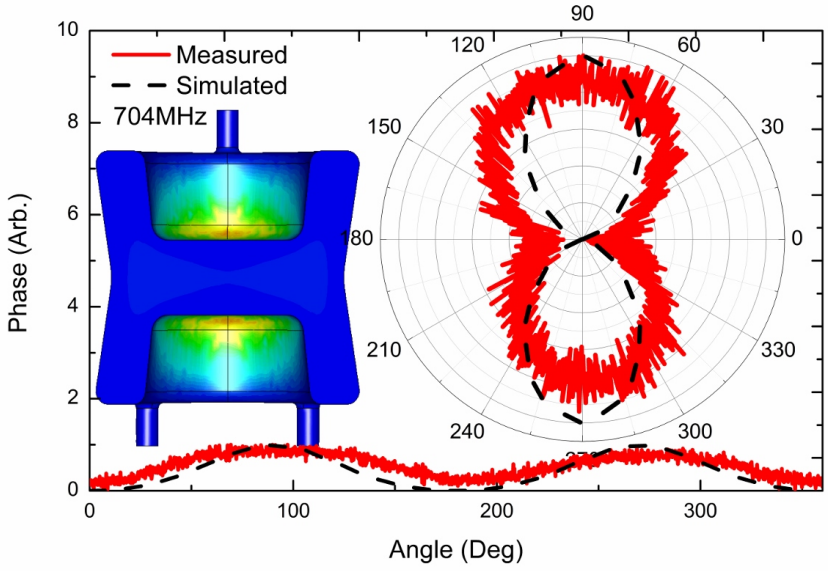

Figure 20: Azimuthal phase profile of the 704MHz mode at the center of the DQWCC. The insets are the transverse cross sectional view of the absolute electric field and the radial plot of the raw data.

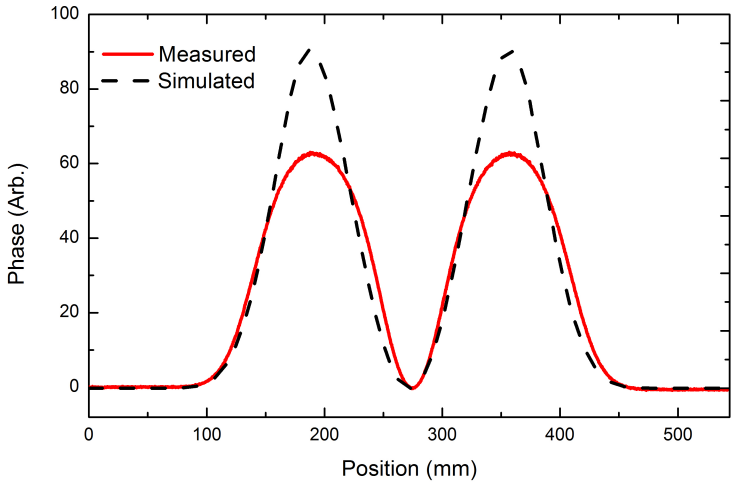

Figure 21: On-Axis longitudinal phase profile of the 755MHz mode.

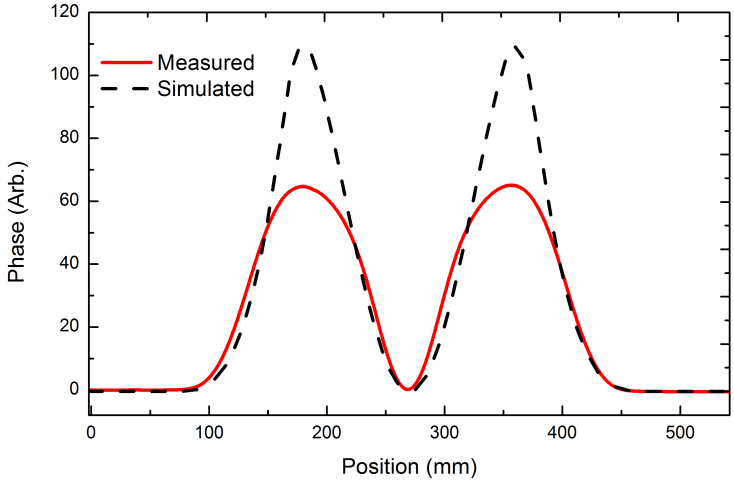

Figure 22: On-Axis longitudinal phase profile of the 755MHz mode 2cm horizontally off axis.

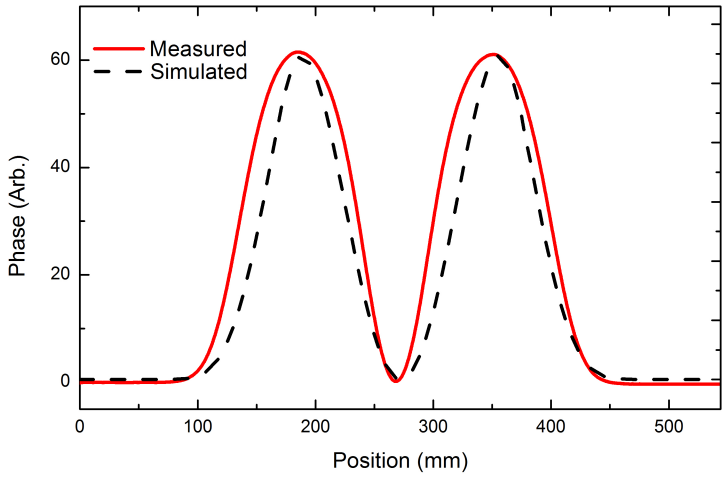

Figure 23: Longitudinal phase profile of the 755MHz mode 2cm vertically off axis.

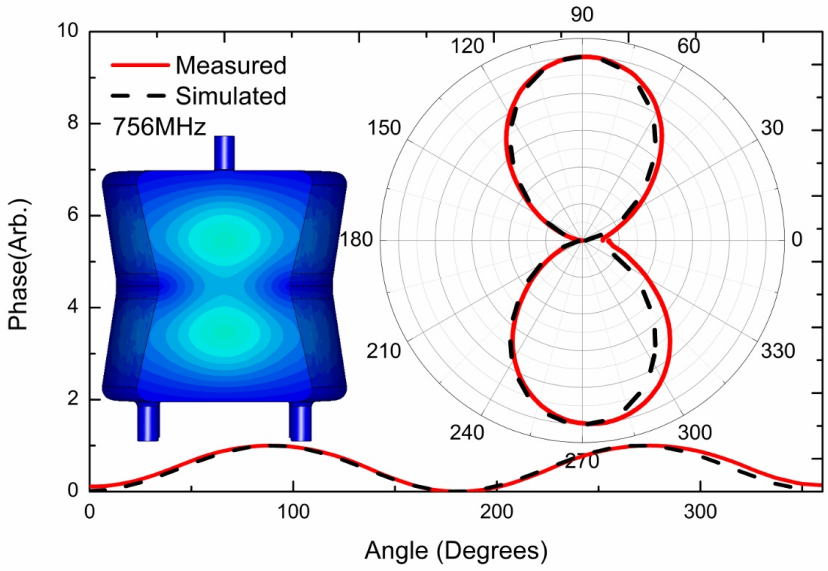

Figure 24: Azimuthal phase profile of the 755MHz mode at the center of the DQWCC. The insets are the transverse cross sectional view of the absolute electric field and the radial plot of the raw data.

3.5 Mode at 800MHz

Due to a software related issue of the automated characterization program longitudinal scans were not performed for this mode. However azimuthal scans were performed and correspond well with simulation. Notice that the field profile shifts 90 degrees when progressing through the cavity which is apparent when looking at the radial plots in Figures 25 and 26. The offset associated with the 0 angle of the azimuthal scan in Figure 25 could attributed to a temperature change or mechanical fluctuations inside the cavity since each measurement took approximately 8 minutes to complete.

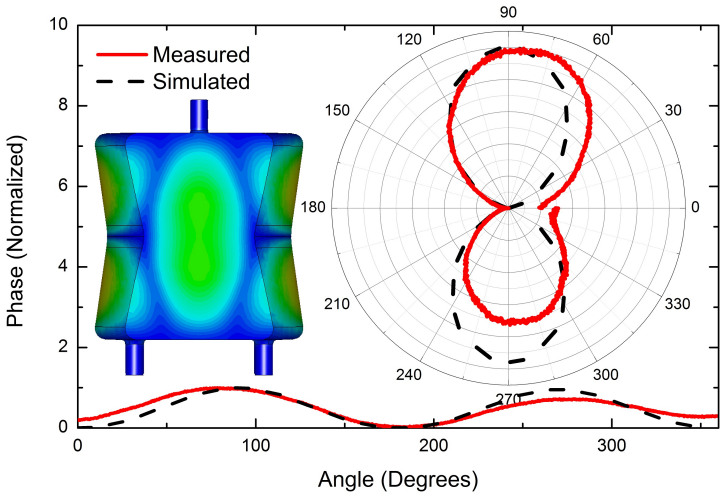

Figure 25: Azimuthal phase profile of the 800MHz mode at $L/4$ of the DQWCC. The insets are the transverse cross sectional view of the absolute electric field and the radial plot of the raw data.

3.6 Mode at 957MHz

Characterization scans for this mode can be found in Figures 27, 28, 29 and 30. The correlation between measurement and simulation is excellent.

3.7 Mode at 1080MHz

Characterization scans for this mode can be found in Figures 31, 32, 33 and 34. Again the correspondence between measurement and simulation is excellent.

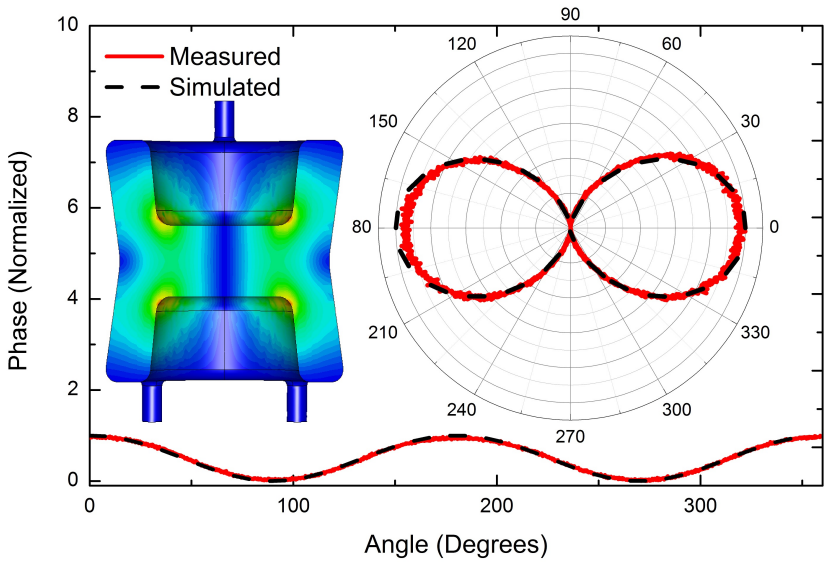

Figure 26: Azimuthal phase profile of the 800MHz mode at the center of the DQWCC. The insets are the transverse cross sectional view of the absolute electric field and the radial plot of the raw data.

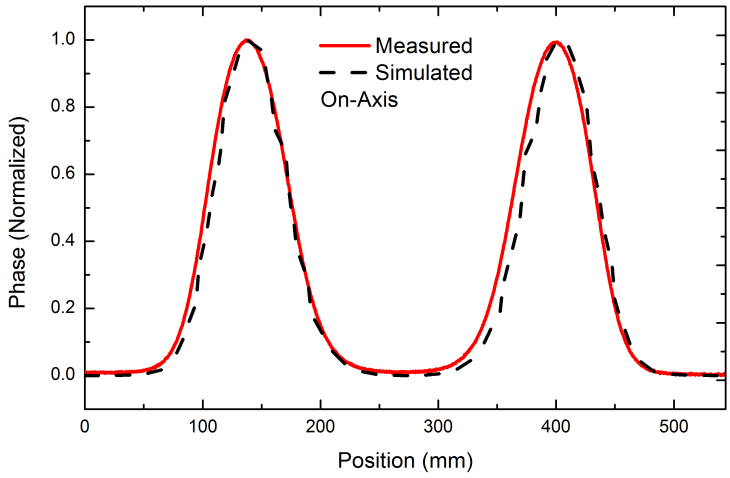

Figure 27: On-Axis longitudinal phase profile of the 957MHz mode.

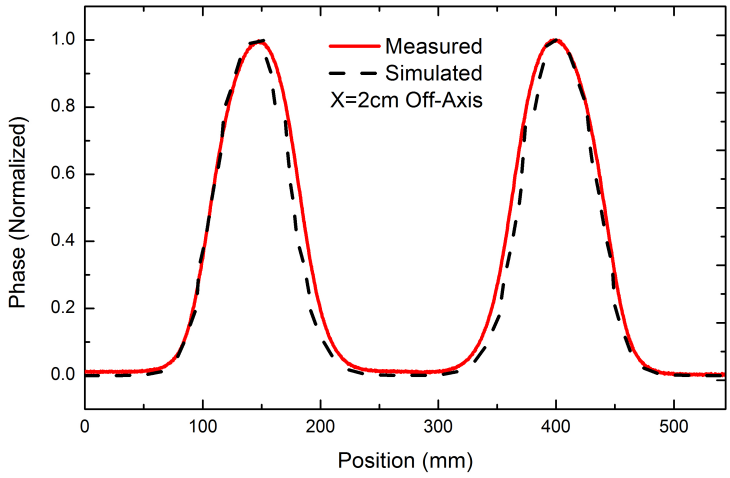

Figure 28: On-Axis longitudinal phase profile of the 957MHz mode 2cm horizontally off axis.

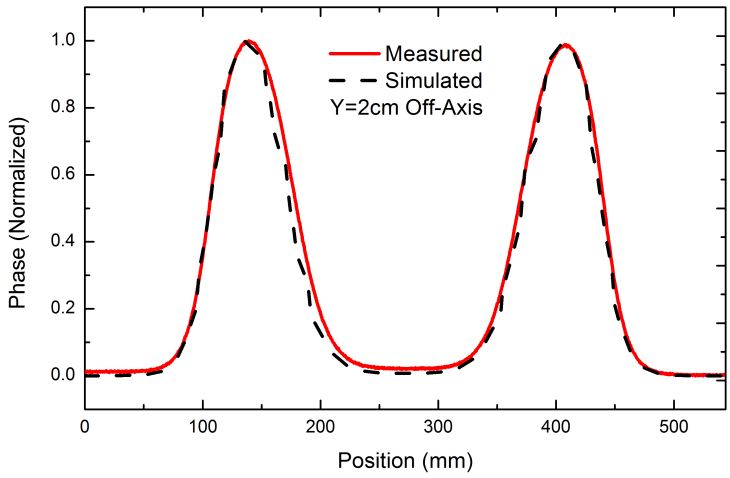

Figure 29: Longitudinal phase profile of the 957MHz mode 2cm vertically off axis.

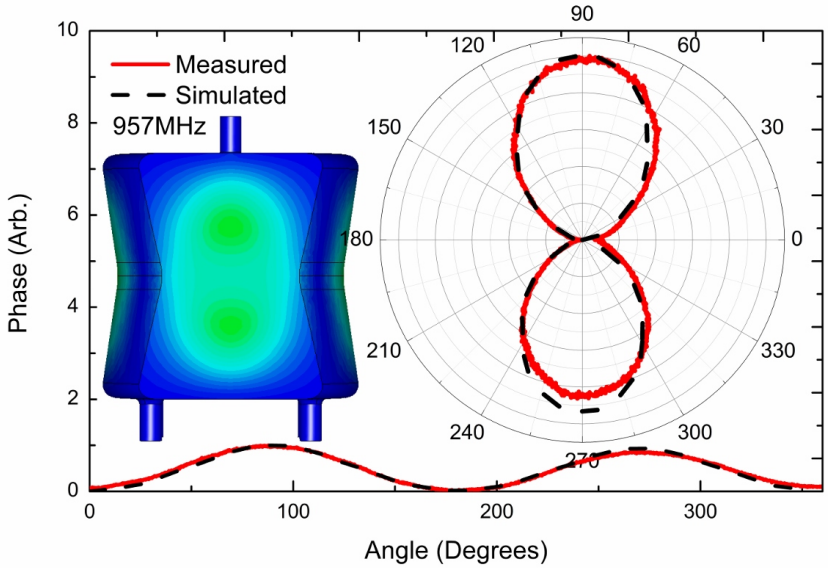

Figure 30: Azimuthal phase profile of the 957MHz mode at $L/4$ of the DQWCC. The insets are the transverse cross sectional view of the absolute electric field and the radial plot of the raw data.

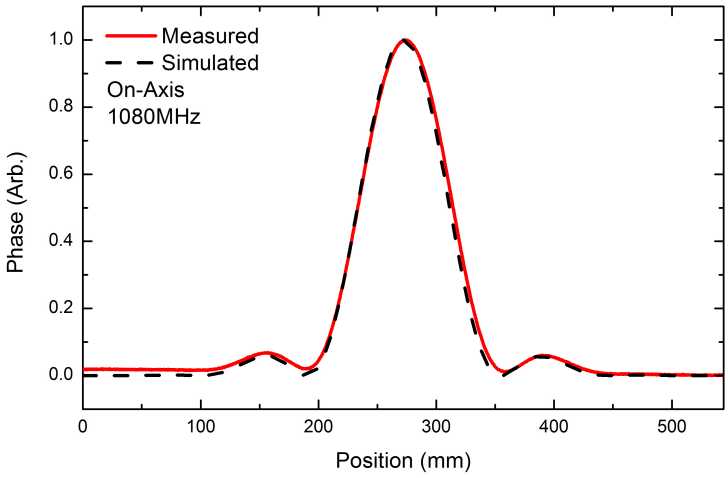

Figure 31: On-Axis longitudinal phase profile of the 1080MHz mode.

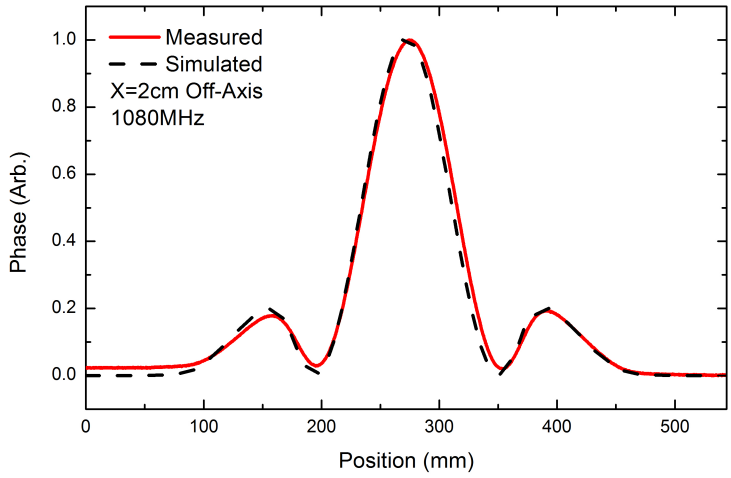

Figure 32: On-Axis longitudinal phase profile of the 1080MHz mode 2cm horizontally off axis.

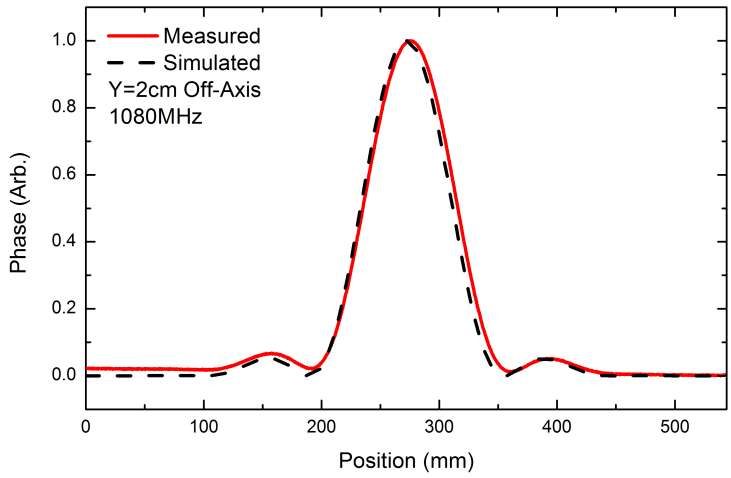

Figure 33: Longitudinal phase profile of the 1080MHz mode 2cm vertically off axis.

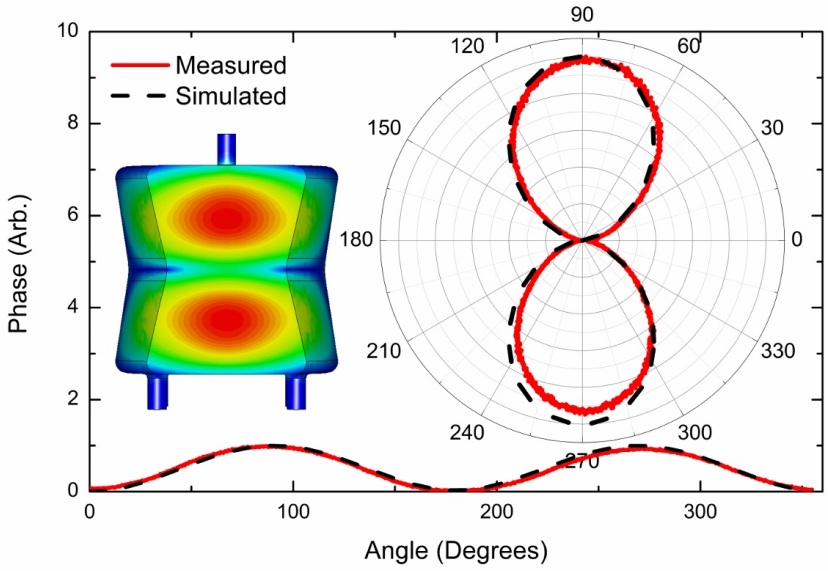

Figure 34: Azimuthal phase profile of the 1080MHz mode at $L/4$ of the DQWCC. The insets are the transverse cross sectional view of the absolute electric field and the radial plot of the raw data.

4 Conclusion

The results of the field profiling measurements yield no surprises when compared to simulated calculations. Despite the obvious misalignment of the crab cavity which gave a parabolic feature to the χ^2 analysis a relatively flat section between -15mm to 15mm suggests excellent consistency and predictability of the crabbing mode with a 99% confidence interval. The efforts of characterizing modes produced direct confirmation of the simulated HOM results. Results of characterized modes up to 2GHz can be found in the network folder mentioned in Section 3.

References

[1] R. Calaga, E. Ciapala, and E. Jensen. *Crab cavities for the lhc luminosity upgrade*. CERN Project Document, August 2010.

[2] B. Xiao, et al. *Design, Prototyping and Cryogenic Testing of a Proof of Principle Double Quarter Wave Crab Cavity*, to be published.

[3] L.C. Maier and J.C Slater. *Field Strength Measurements in Resonant Cavities*. J. Appl. Phys. 23, 68 (1952); doi: 10.1063/1.1701980

[4] C. Marques. *A Comprehensive Investigation and Coupler Design for Higher-Order Modes in the BNL Energy Recovery Linear Accelerator*. Master's thesis, Stony Brook University, 2014.

[5] B. P. Xiao , L. Alberty , S. Belomestnykh , I. Ben-Zvi , R. Calaga , T. Grimm J. Skaritka, Q. Wu, *Mechanical Study of 400MHz Double Quarter Wave Crab Cavity for LHC Luminosity Upgrade*, Proceedings of IPAC, Shanghai, China, 2013